T.2: Physics and applications of semiconductor quantum wells under high magnetic field

Subhomoy Haldar
Semiconductor Materials Lab., Materials Science Section
Homi Bhabha National Institute, Mumbai
Email: subhomoyhaldar.01@gmail.com

Abstract

Semiconductor optoelectronic devices became an integral part of human life due to their excellent physical and chemical properties. In the recent past, challenges that are posed by the unique demand from the variety of directions are being solved by engineering the quantum structures and operating them by the control of external parameters. In this context, we have developed quantum structure-based devices and investigated their unique properties by combining magneto-optical and magneto-transport measurements. Magneto-optical spectroscopy is found to be an excellent tool to probe opto-transport processes and helps in estimating defects acquainted in quantum structures. Unique methods to control recombination and separation of charges by a magnetic field are also demonstrated for device specific applications. Finally, the knowledge of magneto-optical processes in quantum structures is deployed by operating few devices like diode lasers and photo-detectors under a high magnetic field. It is demonstrated that the role of defects and device characteristics can be controlled by an external magnetic field.

1. Introduction

Research on electro-optical properties of III-V semiconductors has provided unprecedented opportunity to develop numerous optoelectronic devices [1,2]. Over the past few decades, a considerable amount of research has been put to develop high efficiency, tunable-wavelength and low-divergent light emitters [3,4]. An extensive research has also been performed to develop high-responsivity photo-detectors with low dark current that can be operated in the harsh environment of radiation [5-7]. The electro-optical properties of these semiconductors can be further enriched by confining charges in a low-dimensional system [e.g., quantum well (QW)]. The impact of charge carrier's confinement on optoelectronic properties has found far-reaching consequences in many of the presently available optoelectronic devices [8]. Besides the structural confinement, a magnetic field driven confinement of charges may also control the spectral linewidth, output power, and operating wavelength of light-emitting devices [9,10]. For example, it has been demonstrated that the efficiency and operating temperature of quantum cascade lasers (QCL) and the response of photodetectors can be increased when subject to a magnetic field [11-13]. More recently, the role of a magnetic perturbation on the performance of single-photon emitters and quantum sensors has been investigated by many authors [14,15]. Moreover, the operation of these advanced optoelectronic devices under a magnetic field can help in optimizing the device configuration to serve future requirements of semiconductor devices.

With this in mind, magneto-optical-transport properties of GaAs-based QWs and their application on semiconductor devices are presented in this article. The impact of quantum confinement, by the internal and external process, on electro-optical properties and effective mass of charge carriers is investigated. It is found that a magnetic field can help suppressing the role of defects on optical processes. A phenomenological model is developed where the field-driven reduction in disorder-related photoluminescence (PL) helps in estimating the defect-density in QWs. Additionally, the competitive mechanism between magnetic confinement and thermal excitation of charges in a QW is studied by combining two complementary magneto-optical spectroscopies. With our interest in correlating optical and transport processes, magneto-optical spectroscopy is also performed in quantum Hall regime. Furthermore, a unique method to control the recombination and separation of electron-hole pairs is demonstrated by an external magnetic field. Finally, to realize the impact of magnetic perturbation on the optoelectronic device efficiency, semiconductor diode lasers and photo-detectors are developed and their properties are investigated under a magnetic field.

2. Experimental details

GaAs-based QWs, their p-i-n photo-detector and diode-laser structures are grown by metal organic vapor phase epitaxy technique (MOVPE). Low-temperature measurements are performed in Janis research cryostat, where the sample/device is kept in a liquid helium bath. The sample space is surrounded by a helical shaped NbTi superconducting magnet, which can produce a magnetic field up to 8 T. For the magneto-PL measurements, a 532 nm green laser is used to excite electrons. Experiments are performed using an optical fiber-based setup, where emission spectra are dispersed by iHR320 spectrometer and detected by Si (or, InGaAs) photo-diode (Figure T.2.1). During surface photovoltage (SPV) measurements and photo-detector testing, a broad spectrum of quartz tungsten halogen lamp is monochromatized by iHR320, which then illuminates the sample (device). Spectroscopic (electrical) measurements are performed by lock-in amplifiers using a mechanical chopper (AC signal), unless otherwise specified. Diode lasers and photo-detectors are fabricated by using a maskless-photolithography system. Details of the setup and steps involved in device development are discussed in Section 7.

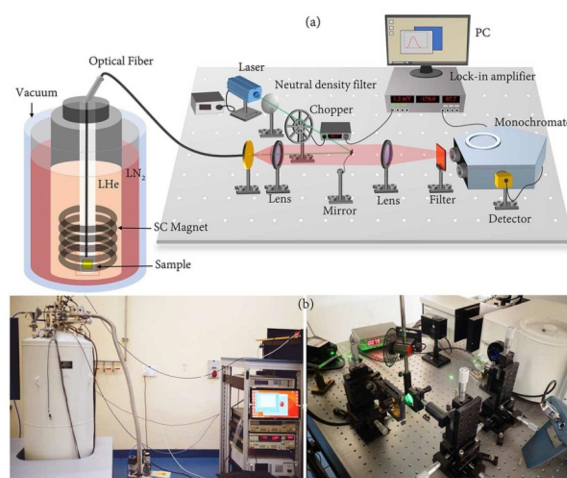

Fig. T.2.1: (a) Schematic and (b) photograph of the low-temperature and high magnetic field measurement setup.

3. Effects of quantum confinement

Even though optical and transport properties of semiconductors can be enriched by confining charge carriers in a QW, penetration of wave function in the surrounding medium upsurges with a reduction in QW thickness. As a result, electron and hole become localized by surface or interface defects. Localization of charges at the hetero interfaces or by point defects plays an important role in determining the performance of a semiconductor device [6]. Such effects of carrier localization can be probed by PL measurements [15], where the recombination via localization centers/trap states causes asymmetry in PL line-shape.

In order to realize the impact of quantum confinement on electro-optical properties, PL spectra are recorded under a magnetic field perpendicular to the sample surface (B_z). Measurements are performed at 4.2 K on a GaAs multiple-QWs structure having four QWs. It is observed that the PL peaks related to the QW-transitions shift towards high energy with an increase in B_z (Figure T.2.2a), which can be attributed to the Landau-diamagnetic and Zeeman energy of electron and hole pairs (i.e., excitons).

$$\Delta\varepsilon = \left(j + \frac{1}{2}\right)\hbar e B_z / \mu^* \pm \frac{1}{2} g \mu_B B_z \qquad (1)$$

Eq. 1 is used to fit the shift in PL peak energy as a function of B_z to estimate reduced mass of excitons, $1/\mu^* = 1/m_e^* + 1/m_h^*$. Here, g is the lande-g factor, μ_B is the Bohr magneton, and m_e^* (m_h^*) is the effective mass of electron (hole). Using the estimated μ^*, binding energy of excitons is evaluated which is $\varepsilon_b = (\mu^* e^4/32\pi^2\hbar^2\varepsilon_0^2\varepsilon_r^2)$. It is found that the estimated μ^* significantly increases with a decrease in QW thickness (Table T.2.1), which cannot be explained by a simple expression of wave function penetration in barrier layers [16]. It is also noticed that a simple picture of parabolic band is not sufficient to explain the higher values of μ^*. Therefore, using the estimated μ^*, non-parabolic band dispersion is evaluated for the four QWs (Figure T.2.2b) [16]. Figure T.2.2b shows that the non-parabolicity of band slightly changes as a result of quantum confinement. In summary, both the band dispersion and exciton binding energy can be altered by quantum confinement. As a result, density of states (absorption coefficient) is modified and non-linear properties start contributing in the photonic processes. Effects of non-linearity and higher ε_b can also be used to enhance the optoelectronic devices efficiency.

Table T.2.1: Effective mass and binding energy of excitons for the Qws

QW thikness (l_w)	μ^*(x m_0)	ε_b(meV)
19 nm	0.114	8.9
10 nm	0.133	10.4
5 nm	0.167	12.7
3 nm	0.178	13.9

3.1. Estimation of point defect density in QWs

A careful observation in Figure T.2.2a shows that the asymmetry in PL peaks, which is attributed to the radiative recombination via defect states, disappears under a high magnetic field. The magnitude of defect related PL (P2) is

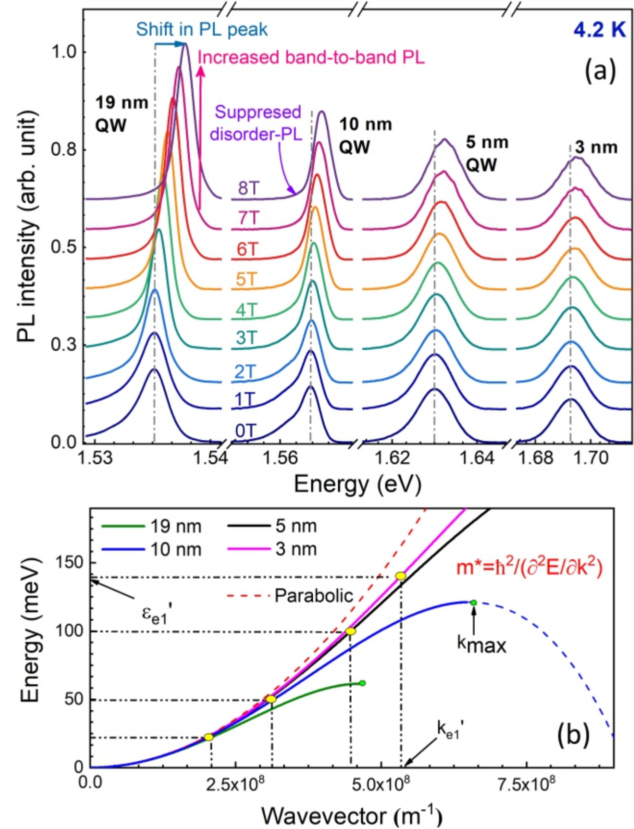

Fig. T.2.2: (a) Magneto-PL spectra of multiple-QWs and (b) their conduction band-dispersion curve.

extracted by fitting PL line-shapes and then plotted in Figure T.2.3a. The decrease in P2 can be correlated by the number of defects experienced by excitons in their spatial extent (Figure T.2.3b). P2 can be expressed as follows:

$$P_2 \sim \left(\frac{4}{3}\right) r_{x,y}^2 r_z \times \delta \qquad (2)$$

Here, the in-plane (out-of-plane) exciton radius is denoted by $r_{x,y}$ (r_z) and point-defect density in QWs is δ. The magnitude of P_2 also depends on dynamical processes governed by the band-to-band recombination (τ_r) and the time required in localizing a charge carrier (τ_c). Hence, the expression for P_2 takes the following form:

$$P_2 = \left(\frac{4}{3}\right) r_{x,y}^2 r_z \times \delta \times \frac{\tau_r}{\tau_c} \qquad (3)$$

The values of τ_r and τ_c for a GaAs QW was previously reported as ~350 ps and ~20 ps, respectively [17,18]. In a high field regime ($B_z \geq B_c$), $r_{x,y} = \sqrt{\hbar/eB_z}$ and hence Eq. 3 becomes [19]:

$$P_2 = \left(\frac{2\hbar l_w}{3eB_z}\right)\delta \times \frac{\tau_r}{\tau_c} \qquad (4)$$

Since charges in the QW are already confined along the growth direction, r_z in Eq. 4 is approximated to the QW thickness (l_w), 2-$r_z \approx l_w$. Thereafter, Eq. 4 is used to fit $P_2(B_z)$ (Figure T.2.3a), and the point defect density in QWs is estimated to be $\delta = (2.3\pm1)\times10^{15}$ cm^{-3} [19].

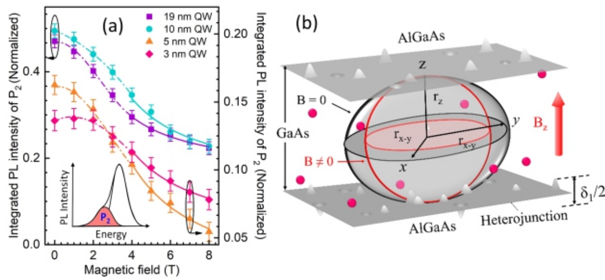

Fig. T.2.3: (a) Disorder-related PL as a function of Bz at 4.2 K and (b) schematic diagram showing spatial confinement of excitons under B_z.

3.2. Magnetic-perturbation on electro-optical processes

Besides the disorder quenching effects, Figure T.2.2a also shows that the PL signal related to band-to-band transition (P_1) increases with B_z. The increase in P_1 can be explained by the in-plane confinement of two oppositely charged particles under B_z, which causes a decrease in τ_r and reduction in inter-subband relaxation time (τ_0). Effects of magnetic field are therefore exploited for successful operation of InGaAs/AlInGaAs QW-based THz QCLs at a higher temperature [12].

To understand the electro-optical processes underlying the performance of those devices, we have performed magneto-PL and magneto-SPV measurements. While PL spectroscopy provides the information related to radiative recombination, SPV gives an evidence of thermal escape of charges from the QW and their drift/diffusion in barrier layers (Figures T.2.4a-b). Therefore, a simultaneous measurement of the two complementary techniques at 100 K helps us to understand magneto-thermal effects in QWs. The temperature for this study is decided from where the binding energy of excitons is nearly equal to the thermal energy (~ 8 meV). Results obtained for a thick and a narrow QW are shown in Figures T.2.4c-d. It is observed that the magnetic confinement of charges enhances the radiative recombination efficiency for the thick QW (19 nm), which is however detrimental for the narrow QW (5 nm). This is because, under a strong B_z, charge carriers escape from the narrow QW. This is also evident from magneto-SPV measurements, where SPV signal related to the narrow QW increases with B_z. The experimental results can also be simulated by a rate equation model considering recombination, relaxation and thermionic escape of charge carriers [20]:

$$\frac{dn_k}{dt} = G_E - \frac{n_k - n_{k+1}}{\tau_0} - \frac{n_k}{\tau_r} + u \times \exp\left(-\frac{\varepsilon_{esc}}{k_B T}\right) \quad (5)$$

Here, G_E denotes the excitation rate of electrons, n_k is for a charge carrier density in k_{th} energy state, and ε_{esc} is the energy required to escape from the QW. Our experiment along with simulated results (Eq. 5) help in predicting the limits of optoelectronic device operation under a high magnetic field [20]. In particular, our investigation provide a clear guideline of the critical QW thickness, which would be essential for a high temperature operation of THz QCL.

4. Magnetic field driven separation of charges for applications related to photovoltaics/sensors

Although the magnetic confinement of charges (Section 3) is

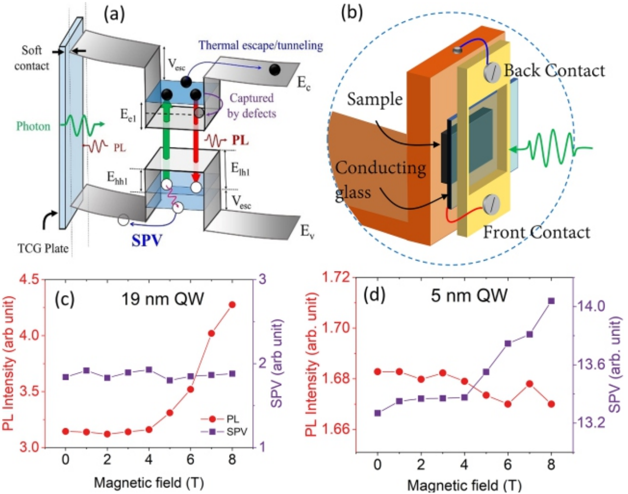

Fig. T.2.4 (a) Generation of PL and SPV in a QW and (b) sample stage design for their simultaneous measurements. PL and SPV signal as a function of B_z for (c) 19 and (d) 5 nm thick QWs at 100 K.

desirous for emission-based devices, a short τ_r is detrimental for photovoltaic applications. To overcome this limitation, we have theoretically shown that electron and hole can be separated by applying a magnetic field parallel to the QW plane (B_y) [21]. Due to this charge separation process, an electric field would be generated at the edges of the QW-sample [$E_x(B_y, V_z)$]. The ability to measure the separation of charges by B_y depends on the quality of heterointerfaces and the distance between the measuring probes, d (Figure T.2.5a). To measure the lateral photovoltage signal from the edges of a device, 10 nos of GaAs QW channels having d=80 μm are fabricated. The channels are connected in series circuit, where each channel acts as a photovoltaic cell under B_y. Therefore, the voltage measurement between the first and last contacts should ideally lead to 10 times higher photovoltage signal than a single channel (Figures T.2.5a-b).

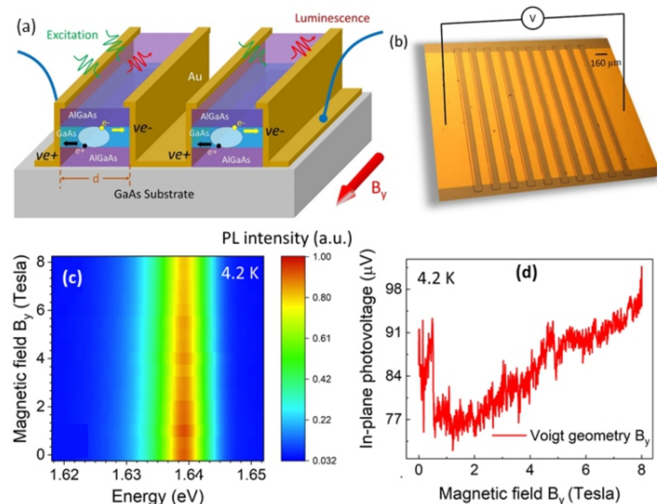

Fig. T.2.5: (a) Schematic and (b) photograph of the fabricated device for lateral-photovoltage measurement. (c) Magneto-PL and (d) lateral magneto- photovoltage signal under B_y.

Magneto-PL spectra and lateral magneto- photovoltage signal are recorded on the strip-like device under B_y (Figures T.2.5c-d). It is observed that the PL signal gradually decreases with an increase in B_y. This indicates that the overlap of electron and hole in the QW decreases. At the same time, lateral photovoltage gradually increases with a rise in B_y (Figure T.2.5d). These observations readily suggest that the separation of electron-hole due to B_y dominates over the confinement of charges in the QW [21]. Here, charge carriers perform a chiral motion across atomically sharp heterointerfaces. Therefore, a long phase coherence length and large spin-dephasing time can be achieved under B_y, which can be useful in novel quantum devices and spintronics applications. In summary, a magnetic field parallel to the QW-plane helps in separating photo-generated charges which is desirous for photovoltaic devices and sensors; whereas a perpendicular field causes a reduction in τ_r and τ_0 which is beneficial for emission-based devices.

5. Magneto-optical spectroscopy in quantum Hall regime

Added to this spectroscopic method, a contact-based magneto-transport measurement is often used to realize electronic processes and scattering mechanism in semiconductors. Despite magneto-resistance measurements processes a paramount of importance in condensed matter physics, contact-based measurements can be a challenge for small, undoped, or multilayered structure. Therefore, we have performed a simultaneous measurement of magneto-optical and quantum Hall measurements to establish correlations between spectroscopic and transport parameters (Figure T.2.6a) [22]. It is observed that the measured magneto-resistances are convoluted with a non-linear background, which is due to parallel layer conduction in the sample (Figure T.2.6b). The variation of R_{xx} and R_{xy} under dark and illuminated conditions are fitted to estimate m_e^* ($0.63m_0$), scattering times (0.9 ps), mobility (1.2×10^5 cm^2/Vs) and carrier density (2×10^{11} cm^{-2}) in the QW. It is also found that the photo-generated holes screen the scattering of electrons, which enhances the mobility of electrons under laser illumination. Under this condition, τ_r, carrier density in Landau states, and Fermi energy as a function of a magnetic field are estimated by magneto-PL spectroscopy [22]. Therefore, the results obtained by combining magneto-PL and magneto-transport measurements provide a complete understanding about the electro-optical processes [22]. In particular, magneto-optical probe is found to be a superior tool to study electronic and optical processes when a contact-based measurement is not feasible.

6. Semiconductor devices under high magnetic field

With this understanding of magnetic field controlled electro-optical processes, we intend to develop semiconductor devices and operate them under B_z.

6.1. Photo-detectors under high magnetic field

Figure T.2.7 shows the layer details and energy band profile of the p-i-n photo-detector [23], where an 18 nm thick GaAs QW is embedded in the i-region. Here, barrier heights of the QW being very small, $\Delta\varepsilon_c$= 97 meV and $\Delta\varepsilon_v$ = 76 meV, a small perturbation due to the magnetic field or thermal energy may influence the carrier escape from the QW.

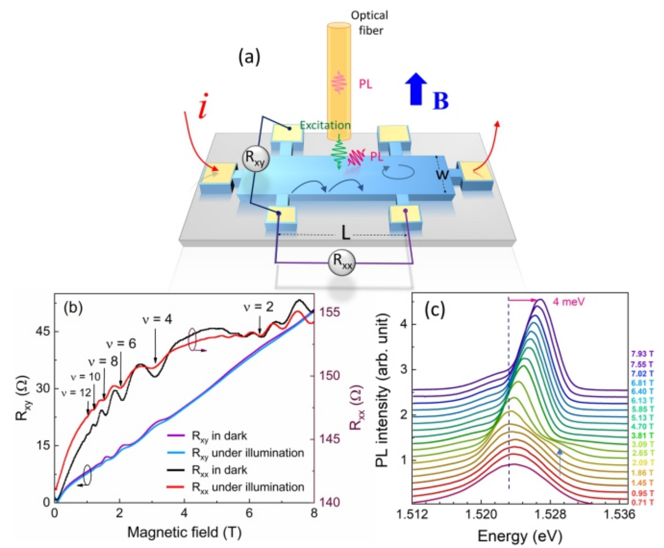

Fig. T.2.6: (a) Simultaneous measurements of Magneto-PL and quantum Hall. (b) Results of magneto transport and (c) magneto-PL measurements at 4.2 K.

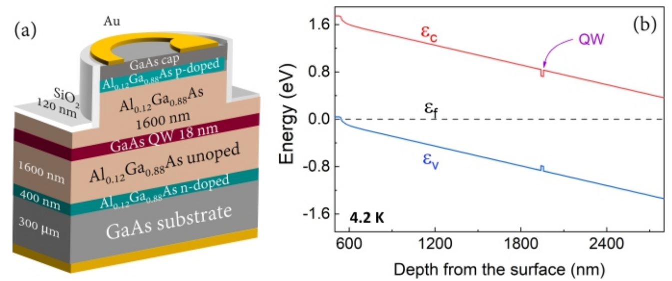

Fig. T.2.7: (a) Layer details and (b) band-profile of the GaAs/AlGaAs p-i-n photo-detector.

Figures T.2.8a-b show the photograph of the fabricated detector and it's current-voltage characteristics in dark and light illumination (λ = 730 nm) at 4.2 K. It is observed that the detector is equally sensitive even for a feeble intensity of light (2 nW). Moreover, the dark current (i_{dark}) of the photo-detector is found to be 10 ±5 pA at -2 V. This extremely low value of i_{dark} can be explained by the accumulation of background charges in the QW-region, which acts as an artificial charge accumulation center. The responsivity of the photo-diode is then estimated by $R=JA_p/p$, [24] where A_p is the active area of the detector, and p is the power of the incident light. The value of R estimated at -6 V is summarized in Table T.2.2. Also, the specific detectivity $D^*=R\sqrt{\{1/[4k_BT/(R'A_e)+2ei_{dark}/A_e]\}}$ and quantum efficiency $\eta^*=R\times hc/e\lambda$ of the device are evaluated with the help of R [25]. Here, $R'A_e$ is the dynamic resistance-area product and A_e being the area of the electric current.

In a separate set of measurement at 83 K, the detector parameters at 210 nW power are estimated to be R = 0.53 A/W, D^* = 1.2×10^{13} $cmHz^{1/2}W^{-1}$, η^*= 0.89 and i_{dark} = 0.5 nA. An increase in R and η^* values at higher temperature can be understood by the activation of charges that were either captured by defect states or confined in the QW region.

Table T.2.2: Responsivity, specific detectivity and quantum efficiency of the photo-detector at 4.2 K

Illumination power (nW)	R (A/W)	D* 10^{13}(cmHz$^{1/2}$W^{-1})	η
2	0.49	2.1	2.83
9	0.45	2.0	0.77
36	0.5	2.2	0.84
210	0.39	1.7	0.66

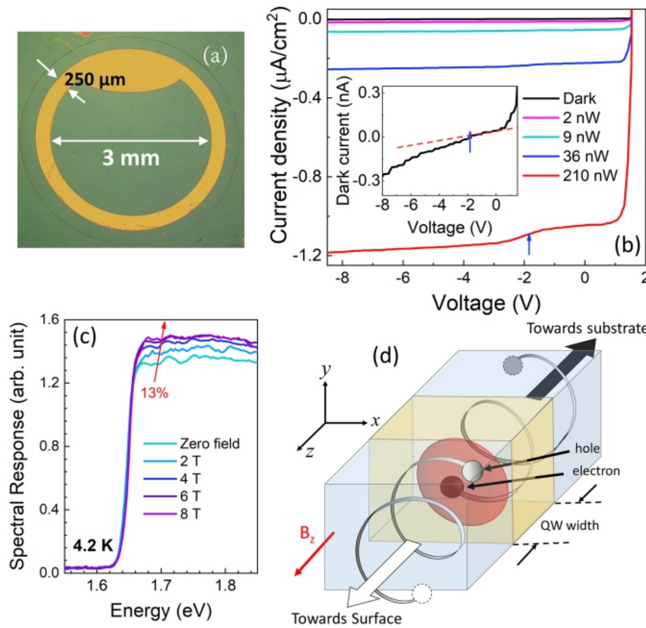

Fig. T.2.8: (a) Photograph of the photo-detector, (b) current-voltage characteristics at different p, and (c) spectral-response as a function of B_z.(d) Magnetic field driven in-plane confinement of charges and their drift due to a built-in electric field.

After that the photo-detector is operated under B_z. The spectral response of the device as a function of B_z is plotted in Figure T.2.8c. It is observed that the response of the device increases by ~13% under B_z = 8 T. Such an observation can be explained as follows:

(i) Diffusion of photo-generated charge carriers in the x-y plane is restricted by B_z. Therefore, the in-plane diffusion followed by the localization (dissipation) of charges decrease. Under this condition, holes and electrons perform a helical motion towards the top and bottom contacts of the device respectively (Figure T.2.8d), which enhances the spectral response under B_z. Notably, the momentum of charge carriers in the x-y plane increases due to B_z, which also helps in faster charge transport along z direction and leads to higher spectral response of the detector.

(ii) In addition, the rate of electron-hole escape from the QW increases due to the magnetic field-driven lowering in the barrier height [20]. These charges then move according to the built-in electric field to enhance the spectral response.

It is therefore evident that carriers confined in QWs can be utilized for photo-detection by an external perturbation, which provides an internal gain in the device. The QW also helps in reducing the dark current. Under a magnetic perturbation, dissipation of charges becomes minimal due to their helical motion and carriers in the QW escape into barrier layer to enhance the spectral response of the detector.

6.2 Diode lasers under high magnetic field

TheInGaAs QW-based diode lasers have been indigenously developed. A schematic of the laser-structure and its energy-band profile are shown in Figure T.2.9.The Laser diode is kept under moderately low operating conditions to avoid any internal temperature drift in the cryogenic system during measurements. They are operated by ILX Lightwave LDP-3840B pulsed current source, where pulse-width PΓ, pulse repetition interval (PRI), and applied current are 4 µs, 0.5 ms, and varied in the range of 0-2.5 A, respectively.

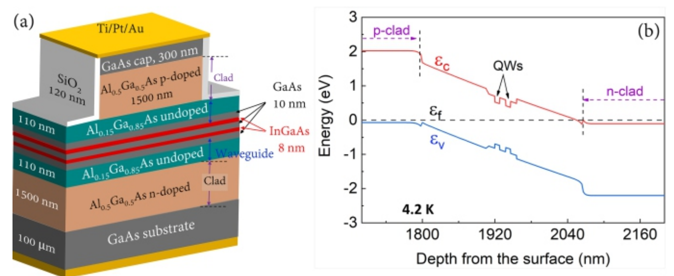

Fig. T.2.9: (a) Schematic and (b) energy band-profile of the InGaAs/GaAs laser structure.

A considerable rise in laser-power is observed with increasing the current at room temperature (Figure T.2.10a). It is observed that the emission spectra isconvoluted with two partially merged lasing features, which are marked as L1 and L2 (Figure T.2.10b). The origin of L2, at lower-energy, is assigned to the electron-hole recombination via defect states. These defects are predominantly originated due to indium-rich valleys in the InGaAs QW [8,26].

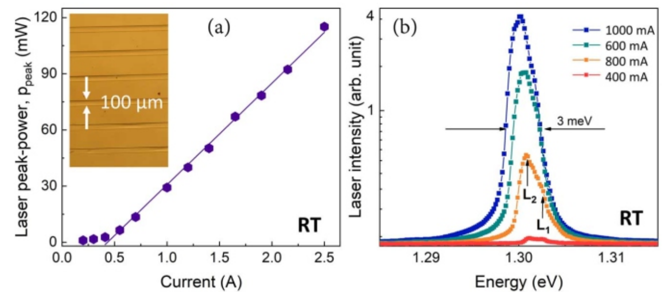

Fig. T.2.10: (a) Light output power-current characteristics, (b) emission spectra of the laser at room temperature.

Thereafter, the device is operated at 4.2 K under B_z. The design of the sample stage for this measurement inside the cryostat is depicted in Figure T.2.11a. Similar to the room temperature operation, laser emission spectra at 4.2 K are convoluted with L_1 and L_2. It is observed that the intensity of L_2 drastically reduces with an increase in B_z, as seen in Figure T.2.11b. The reduction of L_2 can be understood by the magnetic confinement, when carriers in the QW experience a smaller

number of defects. At the same time, the laser intensity related to band-to-band transition (L_1) increases. As a result, lasing peak corresponding to L_1 becomes dominant by suppressing the disorder related feature above 6 T. Therefore, by applying a magnetic field, laser mode can be switched from L_2 to L_1.

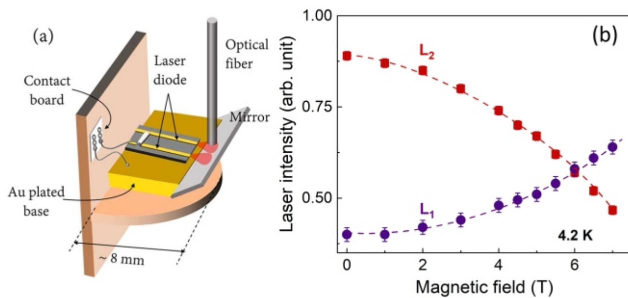

Fig. T.2.11: (a) Sample stage design for the laser operation under a magnetic field, (b) laser intensity related to L_1 and L_2 channels as a function of B_z.

In summary, a magnetic field can help suppressing the laser emission via defect states, which may also offer a tunability in the lasing wavelength. Such an effect would be useful to realize the fundamental mechanisms underlying the wavelength tunability in asymmetric waveguide lasers [27].

7. Experimental setup for device development

7.1. Development of maskless-photolithography setup

One of the essential tools to fabricate semiconductor devices is photolithography. Even though, a mask-based lithography is most suitable for industrial applications, cost and time delay associated in designing and fabricating a photo-mask are some of the major disadvantages. Moreover, there is no further scope of modification once a mask is fabricated.

With this in mind, a maskless-photolithography system is developed at RRCAT using a digital-projector and an optical microscope [28]. The diverging light from a projector is focused by a 10X eye-piece and an objective lens of a microscope. Optical-microscope also allows for the visual inspection of pattern-placement and focusing of light on the substrate (Figures T.2.12a-b). Projector in this setup (1920×1080-pixel resolution) is used to achieve a spatially patterned-light, where the desired image-patterns are drawn in PowerPoint software. Intensity and duration of exposure are controlled by the computer software. An x-y-z-φ controlled stage is used for focusing of incident light and pattern alignment.

A uniform exposure of photoresist is realized throughout the 8×6 mm^2 exposure area having a minimum feature size of ~20 µm. Here, Shipley S1813 photoresist is spin coated on the device at 3500 RPM, which is then baked at 95 °C and exposed for 3 s. The sample is then developed in MF319 for 50 s. Using this setup, laser and detector structures with a variation in size/shape are fabricated (Figures T.2.12c-d), which is now regularly used by the members of Semicond. Mat. Lab., MSS. to pattern numerous device designs.

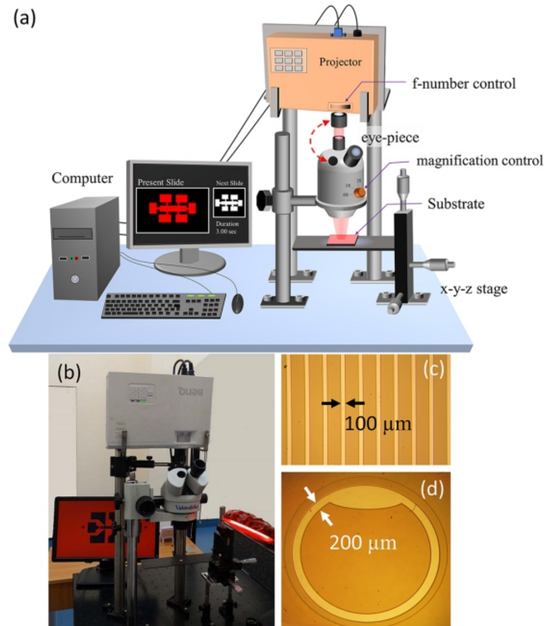

Fig. T.2.12: (a) Schematic and (b) photograph of the maskless-photolithography system. Optical microscope image of (c) diode laser arrays and (d) photo-detector which are developed by the setup.

7.2 Development of photo-detectors

With this flexibility to pattern any device structure and vary device geometry, QW-based photo-detectors are fabricated. In the first step, Au-Ge/Ni/Au is deposited at the back-side of the sample by a thermal evaporator. After that the active area of the detector is defined by the maskless-photolithography setup followed by a chemical etching. To passivate the surface states and to reduce the reflection of photons, a 120 nm SiO_2 is deposited on the surface. Thereafter, a selective area oxide removal is performed and a ring-shaped Schottky contact is made on the top of the detector.

7.3 Development of diode-lasers

$In_{0.2}Ga_{0.8}As$/GaAs double QW-based laser structures are grown on n^+-GaAs substrate.The photolithography technique is used to pattern the sample with 100 µm thick parallel lines of active element. Unwanted areas are chemically etched up to the depth of 1.8 µm, followed by a SiO_2 coating for surface passivation. SiO_2 is selectively removed on top of the active elements and then top contacts are made by Ti/Pt/Au. Finally, the thickness of the sample is reduced to ~100 µm by back-side lapping and polishing, and back-contact is made by Au-Ge/Ni/Au.

8. Conclusion

The impact of charge carrier's confinement on electro-optical properties of QWs, having extremely low disorders, and their applicability on optoelectronic devices development are investigated by magneto-optical- transport measurements. It is found that the role of defects on optical processes in a QW can be suppressed by a magnetic field. Such an effect of disorder quenching is modeled to estimate point defect density by a non-invasive manner. A magnetic field-controlled

recombination and separation of charges is also investigated by complementary magneto-optical spectroscopies, and its utilization in emission-based and photovoltaic devices is elaborated. A magneto-optical probe is found to be an excellent tool to realize electronic processes in quantum structures, which helped in defining the performance of a device under extreme conditions. Finally, the role of a magnetic perturbation on the efficiency of diode-lasers and photo-detectors is investigated. It is shown that the impact of carrier localization on the performance of lasers and photo-detectors can be suppressed by operating the device under a magnetic field; where the magnetic field offers a tunability of device characteristics. To fabricate these devices, a maskless-photolithography setup is also developed, which can pattern a minimum feature size of ~ 20 μm.

Acknowledgements

The research work presented here is a brief summary of the Ph. D. thesis work of Mr. Subhomoy Haldar which is performed under the supervision of Prof. V.K. Dixit. Author acknowledges Prof. V.K. Dixit for the scientific discussions, guidance, encouragement and support during the entire work. Author also acknowledges Ms. G. Vashisht, Mr. R. Roychowdhury, Dr. S.K. Khamari for fruitful scientific discussions and Mr. S. Porwal, Mr. U.K. Ghosh, Mr. A. Jaiswal and Mr. A. Khakha for their experimental supports. Mr P. K. Kush and his team are acknowledged for providing liquid Helium. Author is thankful to Dr. T.K. Sharma, Head, Materials Science Section for scientific discussions along with encouragement and support.Mr. S.V. Nakhe, Director, RRCAT and Mr. Debashis Das, former Director, RRCAT are specially acknowledged for their constant support during this work and HBNI-RRCAT for providing the research fellowship.

References

[1] N. Li et al. “Ultra-low-power sub-photon-voltage high efficiency light-emitting diodes” Nat. Photonics **13**, 588 (2019).

[2] B.E. Kane, L.N. Pfeiffer, & K.W. West. "High mobility GaAs heterostructure field effect transistor for nanofabrication in which dopant ‐ induced disorder is eliminated." Appl.Phys.Lett.**67**, 1262 (1995).

[3] D. A. Veselov, K. R. Ayusheva, N. A. Pikhtin, A. V. Lyutetskiy, S. O. Slipchenko, & I. S. Tarasov, “Two-state operation of high-power semiconductor lasers with a thick quantum well” J. Appl. Phys. **121**, 163101 (2017).

[4] A.F. Castiglia, M. Rossetti, D. Marcus, & C. Velez, “Low power edge-emitting laser diode and laser diode module”, US Patent 10,193,310 (2019).

[5] R.M. France et al., “Development of Lattice- Mismatched GaInAsP for Radiation Hardness” IEEE Journal of Photovoltaics **10**, 103 (2019).

[6] G. Vashisht, V.K. Dixit, S. Porwal, R. Kumar, T.K. Sharma, & S.M. Oak, “Charge carrier localization effects on the quantum efficiency and operating temperature range of InAsxP1−x/InP quantum well detectors” J. Appl. Phys. **119**, 095708 (2016).

[7] V.K. Dixit et al, “Effect of high dose γ-ray irradiation on GaAs pin photodetectors” Nucl. Instrum. Methods Phys. Res. **785**, 93 (2015).

[8] V.K. Dixit et al., “Evaluation of structural and microscopic properties of tetragonal ZrO2 for the facet coating of 980 nm semiconductor laser diodes” J. Phys. D: Appl. Phys. **48**, 105102 (2015).

[9] Y. Arakawa, K. Vahala, A. Yariv, & K. Lau, “Reduction of the spectral linewidth of semiconductor lasers with quantum wire effects—Spectral properties of GaAlAs double heterostructure lasers in high magnetic fields” Appl. Phys. Lett. **48**, 384 (1986).

[10] D. Beznosko, G. Blazey, A. Dyshkant, V. Rykalin, & V. Zutshi, “Effects of the strong magnetic field on LED, extruded scintillator and MRS photodiode” Nucl. Instrum. Methods Phys. Res. **553**, 438 (2005).

[11] A. Wade et al. “Magnetic-field-assisted terahertz quantum cascade laser operating up to 225 K” Nat. Photon.**3**, 41 (2009).

[12] F. Valmorra, G. Scalari, K. Ohtani, M. Beck, & J. Faist, “InGaAs/AlInGaAs THz quantum cascade lasers operating up to 195 K in strong magnetic field”. New J. of Phys. **17**, 023050 (2015).

[13] C. Yu, L. Li, T.F. Xu, B. Zhang, X. Luo, & W. Lu, “Strong terahertz response in quantum well photodetector based on intradonor transition by magnetic field” AIP Advances **8**, 125014 (2018).

[14] S. Komiyama, O. Astaev, V. Antonov, T. Kutsuwa, & H. Hirai, “A single-photon detector in the far-infrared range” Nature **403**, 405 (2000).

[15] V.K. Dixit, S. Porwal, S.D. Singh, T.K. Sharma, S. Ghosh, & S.M. Oak, “A versatile phenomenological model for the S-shaped temperature dependence of photoluminescence energy for an accurate determination of the exciton localization energy in bulk and quantum well structures” J. Phys. D Appl. Phys. **47**, 065103.

[16] S. Haldar et al., “Effect of carrier confinement on effective mass of excitons and estimation of ultralow disorder in AlGaAs/GaAs quantum wells by magneto-PL” Sci. Rep. **7**, 1 (2017).

[17] T. Damen, J. Shah, D. Oberli, D. Chemla, J. Cunningham, & J. Kuo, “Dynamics of exciton formation and relaxation in GaAs quantum wells” Phys. Rev. B **42**, 7434 (1990).

[18] M. Gulia, F. Rossi, E. Molinari, P.E. Selbmann, and P. Lugli, “Phonon-assisted exciton formation and relaxation in GaAs/As quantum wells” Phys. Rev. B **55**, R16049 (1997).

[19] S. Haldar, V.K. Dixit, G. Vashisht, S. Porwal, & T.K. Sharma, “The effect of magnetic field on free and bound exciton luminescence in GaAs/AlGaAs multiple quantum well structures: a quantitative study on the estimation of ultra-low disorder” J. Phys. D. Appl. Phys. **50**, 335107 (2017).

[20] S. Haldar, V.K. Dixit, G. Vashisht, S. Porwal & T.K. Sharma, “Radiative and non-radiative recombination of thermally activated magneto-excitons probed via quasi-simultaneous photoluminescence and surface-photovoltage spectroscopy” J. Appl. Phys. **124**, 055704 (2018).

[21] S. Haldar, A. Banerjee, G. Vashisht, S. Porwal, T.K. Sharma & V.K. Dixit, “A parallel magnetic field driven confinement versus separation of charges in GaAs

quantum well investigated by magneto-photovoltage and magneto photoluminescence spectroscopy" J. Lumin **206**, 342 (2019)

[22] S. Haldar, G. Vashisht, S. Porwal, T.K. Sharma & V.K. Dixit "Simultaneous magneto-electro-optical measurements in modulation-doped quantum well: An investigation on magneto-PL intensity oscillations". J. Appl. Phys. **125**, 205701 (2019).

[23] M. Group, Band engineering, http://my.ece.ucsb.edu/mgrundmann/bandeng.htm

[24] M.K. Das & N. Das, "Calculating the responsivity of a resonant-cavity-enhanced SiGe/Si multiple quantum well photodetector" J. Appl. Phys. **105**, 093118 (2009).

[25] P. Martyniuk et al., "Mid-wave T2SLs InAs/GaSb single pixel PIN detector with GaAs immersion lens for HOT condition" Solid-State Electronics **119**, 1 (2016).

[26] V.K. Dixit et al., "Investigation into the complexities in active region of quantum well laser diode arrays" Kiran 27 (2016).

[27] D.A. Veselov et al., "Two-state operation of high-power semiconductor lasers with a thick quantum well" J. Appl. Phys. **121**, 163101 (2017).

[28] S. Haldar et al., "Development of a simple cost effective maskless-photolithography system" AIP Conference Proceedings, **2115**, 030219 (2019).

MOVPE facility for growth of semiconductor quantum structures.